A nonsmooth progress function algorithm for frequency shaping control design

Journal:	*IET Control Theory & Applications*
Manuscript ID:	CTA-2007-0183.R2
Manuscript Type:	Research Paper
Date Submitted by the Author:	n/a
Complete List of Authors:	Simões, Alberto; ONERA-CERT, DCSD Apkarian, Pierre; ONERA-CERT, DCSD Noll, Dominikus; Université Paul Sabatier, Institut de Mathématiques
Keyword:	H-infinity synthesis, multidisk problems, structured controller design, nonsmooth optimization, flexible systems, large size systems

A nonsmooth progress function algorithm for frequency shaping control design

Alberto M. Simões * Pierre Apkarian † Dominikus Noll ‡

Abstract

In classical controller design, closed-loop performance specifications arise naturally as constraints on restricted frequency bands. This leads to a difficult design problem, which is currently circumvented by heuristic techniques. In this paper, we develop a nonsmooth progress function algorithm which enjoys features similar to exact penalization strategies to solve the problem. This allows us to compute locally optimal solutions to the frequency shaping control design problem. The new technique is highly efficient, as we demonstrate by way of two case studies, a large dimension power system, and a flexible telescope.

Keywords: H_∞-synthesis, multidisk problems, structured controller design, nonsmooth optimization, power systems, flexible systems, large size systems.

*ONERA-CERT, Centre d'études et de recherche de Toulouse, Control System Department, 2 av. Edouard Belin, 31055 Toulouse, France - Email: alberto.simoes@cert.fr - Fax: +33 5.62.25.27.64.

†ONERA-CERT, Centre d'études et de recherche de Toulouse, Control System Department, 2 av. Edouard Belin, 31055 Toulouse, France - and - Université Paul Sabatier, Institut de Mathématiques, Toulouse, France - Email: apkarian@cert.fr - Tel: +33 5.62.25.27.84 - Fax: +33 5.62.25.27.64.

‡Université Paul Sabatier, Institut de Mathématiques, 118, route de Narbonne, 31062 Toulouse, France - Email: noll@mip.ups-tlse.fr - Tel: +33 5.61.55.86.22 - Fax: +33 5.61.55.83.85.

1 Introduction

Frequency shaping control design consists in the simultaneous minimization of a finite family of closed-loop performance functions

$$f(K) = \max_{i=1,\ldots,N} \|T_{w^i \to z^i}(K)\|_{I_i}, \tag{1}$$

where K stands for the feedback controller, $s \mapsto [T_{w^i \to z^i}(K)](s)$ is the ith closed-loop performance channel, and $\|T_{w^i \to z^i}(K)\|_{I_i}$ denotes the peak value of the transfer function maximum singular value norm on a prescribed frequency interval I_i:

$$\|T_{w^i \to z^i}(K)\|_{I_i} = \sup_{\omega \in I_i} \overline{\sigma}\left([T_{w^i \to z^i}(K)](j\omega)\right).$$

The frequency band I_i is typically a closed interval $I_i = [\omega_1^i,\, \omega_2^i]$, or more generally, a finite union of intervals $I_i = [\omega_1^i,\, \omega_2^i] \cup \ldots \cup [\omega_{q_i}^i,\, \omega_{q_{i+1}}^i]$, where right interval tips may take infinite values.

Multi-band control design is of great practical interest since performance criteria are often expressed as constraints on specific frequency bands. Currently these bands are handled indirectly by introducing weighting functions. This is inconvenient since finding appropriate weighting functions is time-consuming and always prone to failure, and also because this increases the plant order and thereby the controller order. Our approach dispenses with weighting functions and avoids the indicated difficulties.

Despite its importance, only very few methods for multi-band synthesis are reported in the literature. In [14], an extension of the Kalman-Yakubovich-Popov Lemma [18] is developed for band restricted frequency domain constraints, but a fairly conservative convexifying procedure is adopted. The QFT method [13] may be used to solve band limited synthesis problems, but it is no longer suited if additional structural constraints on the controller have to be satisfied. Similar comments could be made about synthesis based on the Youla parametrization, which generally leads to high-order controllers [9]. Other tools, as the classical Bode, Nyquist and Nichols plots [7,12], and more recently [20], are suited for this type of application, but are essentially limited

to single-input single-output systems, even though some multivariable generalizations have been attempted over the years [15].

Our new multi-band synthesis algorithm is based on a nonsmooth optimization technique. One of its principal features is that a substantial part of the computations is carried out in the frequency domain. This allows efficient function and gradient calculations and avoids Lyapunov variables, whose number grows quadratically with the system size. The latter is one of the principal difficulties of approaches based on linear or bilinear matrix inequalities.

The algorithm proposed here expands on the nonsmooth H_∞ synthesis method of [3]. It does not require the management of penalty or homotopy parameters, as was still necessary in [5]. The technique in reference [5] is based on a penalization strategy, which essentially constructs a modified objective function augmented by a penalty term of the constraint violation. Despite its simplicity and intuitive appeal penalization and barrier strategies raise important and critical questions as: how to initialize and update the penalty parameter? how to avoid the inherent ill-conditioning of these techniques for asymptotic values of the penalty parameter? These issues make the implementation of these techniques a rather difficult task. Moreover, these strategies may lead to unsatisfactory execution times since an unconstrained nonlinear problem must be solved to completion for each value of the penalty (barrier or homotopy) parameter.

The strategy proposed in the present work is more in line with exact penalization techniques where solutions to the original problem are obtained with a single execution with fixed value of the penalty parameter. In the paper, a progress function is introduced which plays the role of an exact penalty function and computing local solutions reduces to minimizing the progress function.

It is also important to notice that in contrast with H_∞-synthesis [3], in multi-band synthesis closed-loop stability has to be modelled as a mathematical programming constraint, if the frequency bands used for performance do not fully cover the frequency axis in a sense that will be clarified in the application section.

In order to demonstrate the efficiency of our nonsmooth design technique in practically difficult cases, two benchmark studies are presented. The first example is a power system, which is challenging because of the large dimension. For such large-scale systems, model reduction is

typically used, but bears the risk of having to work with overly simplified reduced models. Our new approach is versatile in this situation, because it allows to synthesize structured controllers such as reduced-order or decentralized controllers, or controllers including washout filters.

The second case study is a flexible telescope system, where frequency-domain constraints arise naturally due to the presence of flexible modes. In general, performance is dominant in the low frequency range, while stability and robustness have to be guaranteed in the high frequency range. In contrast with the traditional approach, where the plant and weighting functions are assembled into an unique synthesis interconnection $w \to z$, our approach allows to keep each frequency band constraint $w^i \to z^i$ explicitly, and to address the problem in a direct and natural way.

The structure of the paper is as follows. Section 2 provides a precise statement of the multi-band frequency domain design problem. Our resolution technique based on a nonsmooth algorithm is discussed in section 3. Two realistic case studies are presented in section 4.

Notation

Let $\mathbb{R}^{n\times m}$ be the space of $n\times m$ matrices, equipped with the corresponding scalar product $\langle X, Y\rangle = X \bullet Y := \mathrm{Tr}(X^T Y)$, where X^T is the transpose of the matrix X, $\mathrm{Tr}X$ its trace. For complex matrices, X^H denotes the conjugate transpose. For Hermitian or symmetric matrices, $X \succ Y$ means that $X - Y$ is positive definite, $X \succeq Y$ that $X - Y$ is positive semi-definite. The symbol $\mathbb{H}^m$ stands for the set of Hermitian matrices of size m. We let λ_1 denote the maximum eigenvalue of a symmetric or Hermitian matrix. The notation $\mathrm{co}(S)$ refers to the convex hull of the set S. The notation $\|.\|$ stands for the max singular value norm $\overline{\sigma}$, unless stated otherwise. We shall use concepts from nonsmooth analysis covered by [11]. In particular, for a locally Lipschitz function $f : \mathbb{R}^n \to \mathbb{R}$, $f'(x, d)$ denotes the Clarke directional derivative of f at x in the direction d defined as

$$f'(x,d) := \limsup_{\substack{y\to x\\ t\to 0\\ t>0}} \frac{f(y+td)-f(y)}{t}.$$

The notation $\partial f(x)$ denotes the Clarke subdifferential of f at x defined as

$$\partial f(x) := \{s \in \mathbb{R}^n : \langle s, d\rangle \leq f'(x,d), \forall d \in \mathbb{R}^n\}.$$

For functions of two variables $f : \mathbb{R}^n \times \mathbb{R}^m \to \mathbb{R}$, the notation $\partial_1 f(x,y)$ is used to denote its Clarke subdifferential with respect to x at (x,y). In the sequel of the paper, each $T_{w^i \to z^i}$ is a smooth operator defined on the open domain $\mathcal{D} \subset \mathbb{R}^{(m_2+k)\times(p_2+k)}$ of kth order stabilizing feedback controllers

$$K := \begin{bmatrix} A_K & B_K \\ C_K & D_K \end{bmatrix},\ A_K \in \mathbb{R}^{k\times k}$$

with values in the infinite dimensional space RH_∞ of rational stable transfer function matrices.

2 Multi-band frequency domain design

We consider a plant P in state-space form

$$P(s) : \begin{bmatrix} \dot{x} \\ y \end{bmatrix} = \begin{bmatrix} A & B \\ C & D \end{bmatrix} \begin{bmatrix} x \\ u \end{bmatrix}$$

together with N concurring performance specifications, represented as a family of plants $P^i(s)$ described in state-space form as

$$P^i(s) : \quad \begin{bmatrix} \dot{x}^i \\ z^i \\ y^i \end{bmatrix} = \begin{bmatrix} A^i & B_1^i & B_2^i \\ C_1^i & D_{11}^i & D_{12}^i \\ C_2^i & D_{21}^i & D \end{bmatrix} \begin{bmatrix} x^i \\ w^i \\ u^i \end{bmatrix},\ i = 1,\ldots,N, \tag{2}$$

where $x^i \in \mathbb{R}^{n^i}$ is the state vector of P^i, $u^i \in \mathbb{R}^{m_2}$ the vector of control inputs, $w^i \in \mathbb{R}^{m_1^i}$ the vector of exogenous inputs, $y^i \in \mathbb{R}^{p_2}$ the vector of measurements and $z^i \in \mathbb{R}^{p_1^i}$ the controlled or performance vector associated with the ith input w^i. The performance channels typically incorporate frequency filters which create new states x^i containing the state x of P, so that the

matrices A^i contain the original system matrices A, etc. The difference with the usual multi-channel synthesis is that each $T_{w^i \to z^i}$ is only tested on a specific frequency band I_i. For simplicity of the presentation, we have assumed throughout that $D = 0$. When this does not hold, we tacitly assume either a standard loop transformation of the controller is performed afterwards [21, p.317] or subgradient formulas are suitably extended to a non-zero feedthrough plant matrix.

The multi-band synthesis problem consists of designing a dynamic output feedback controller $u^i = K(s)y^i$ for the plant family (2) that stabilizes the original plant P in closed-loop and that minimizes, among all internally stabilizing controllers, the worst case performance function (1). In formulas:

$$\begin{array}{ll} \text{minimize} & f(K) = \max\limits_{i=1,\ldots,N} \|T_{w^i \to z^i}(K)\|_{I_i} \\ \text{subject to} & K \text{ stabilizes } (A, B, C) \end{array} \tag{3}$$

where the case $k = 0$ of a static controller $K(s) = D_K$ is included. Often practical considerations require additional structural constraints on the controller K. Structures as low-order controllers ($0 \leq k \ll n_i$), decentralized or fixed pattern controllers, PID control, and much else are easily incorporated into program (3) as nonlinear programming constraints, see [2] for details.

A difficulty in (3) is that stability is not a constraint in the usual sense of mathematical programming, because the set $\mathcal{D}$ of closed loop stabilizing K is open, and an element K on the boundary $\partial\mathcal{D}$ is *not* a valid solution of the control problem. Since an optimization algorithm for (3) eventually converges to a solution on the boundary of $\mathcal{D}$, we have to modify this constraint in order to avoid numerical failure. One way to do this is to replace program (3) by

$$\begin{array}{ll} \text{minimize} & f(K) = \max\limits_{i=1,\ldots,N} \|T_{w^i \to z^i}(K)\|_{I_i} \\ \text{subject to} & g(K) = \|(sI - \mathcal{A}(K))^{-1}\|_\infty - \beta^{-1} \leq 0 \end{array} \tag{4}$$

where $\mathcal{A}(K)$ is the closed-loop system matrix, and β is a small parameter. Note that the constraint $g(K) \leq 0$ in (4) will force the controller iterates to remain in the stabilizing region in the course of the algorithm. The value of $\beta > 0$ is the smallest distance to instability we allow the closed-loop

system [10]. In our experiments we usually choose $\beta \approx 10^{-9}$.

Another practically interesting cast is the following

$$\begin{aligned} \text{minimize} \quad & f_1(K) = \|T_{w^1 \to z^1}(K)\|_{I_1} \\ \text{subject to} \quad & f_i(K) = \|T_{w^i \to z^i}(K)\|_{I_i} - \gamma_i \leq 0, \quad i = 2, \ldots, N \\ & g(K) = \|(sI - \mathcal{A}(K))^{-1}\|_\infty - \beta^{-1} \leq 0 \end{aligned} \tag{5}$$

where one performance channel is minimized subject to performance constraints on the other channels. Both formulation (4) and (5) are equivalent as soon as appropriate scalars α_i are introduced to weigh the relative importance of the channels in (4). In the numerical experiments of section 4 we have chosen to work with (4), although our algorithm is open to the option (5).

We note that (4) and (5) are nonconvex programs, and finding a global solution is difficult as a rule. In response, the technique we propose here is a local optimization method, which is less ambitious than global methods, providing solutions with a local optimality certificate. If the computed locally optimal controller turns out to be unsatisfactory, we have to restart our method at a different initial controller or to re-tune the weights between the various performance objectives. Our numerical experiments in Section 4 show that the slight inconvenience of a local method is largely compensated by its practical benefits in terms of controller structure, flexibility to manage a set of conflicting specifications, and of cpu time.

The strategy we adopt to select the individual weights in (4) for the benchmark studies of Section 4 is analogous to the aspiration levels approach for multi-objective optimization, see [9, p.64]. We first normalize $f(K)$ in (4) by setting

$$f(K) = \max_{i=1,\ldots,N} \|T_{w^i \to z^i}(K)\|_{I_i}/\gamma_i,$$

where each γ_i represents the aspiration level for the ith channel. The goal then becomes to find a solution with $f(K) \leq 1$, which indicates whether our specifications have been met. We then perform a few trial-and-error designs where satisfied constraints can be strengthened while violated constraints can be relaxed.

3 Nonsmooth minimization technique

In this section we give a concise presentation of our optimization method. For a more detailed introduction to the salient features we refer the reader to [3, 17], and to [16] for variations of the present technique. Our goal is to minimize a function of the form

$$f(K) = \max_{i=1,\dots,N} f_i(K),$$

where each $f_i(K)$ is a nonsmooth and nonconvex function of the form

$$f_i(K) = \sup_{\omega\in[\omega_{i1},\omega_{i2}]} \lambda_1([T_{w^i\to z^i}(K)](j\omega)[T_{w^i\to z^i}(K)](j\omega)^H).$$

Notice that for convenience we have replaced f, f_i, g in (4) and (5) by their squares. In order to alleviate notation, we will henceforth write $f_i(K,\omega) = \lambda_1([T_{w^i\to z^i}(K)](j\omega)[T_{w^i\to z^i}(K)](j\omega)^H)$, $T_i := T_{w^i\to z^i}$, and $[S_i(K)](j\omega) = [T_{w^i\to z^i}(K)](j\omega)[T_{w^i\to z^i}(K)](j\omega)^H$. The remainder of this section is now dedicated to the following three issues. How to compute function values and subgradients of $f(K)$ and $g(K)$, how to use this information to generate steps which reduce the value of f and render the constraint $g(K) \le 0$ feasible, and finally, how to assemble this into a numerically successful first-order algorithm.

3.1 Computing jet information

Computing function values of each $f_i(K)$ can be based on the Hamiltonian algorithm of [8], originally designed to compute the H_∞ norm of a stable transfer function. The original technique can be applied with minor changes to the case where the search for imaginary-axis Hamiltonian eigenvalues is restricted to the frequency band of interest. A numerical issue may arise when the dichotomy search hits function values at infinity, $f_i(K,\infty)$. We can get around this difficulty by mapping the ith frequency band $[\omega_{i1},\omega_{i2}]$ conformably onto $[0,\infty]$ via

$$\omega' = \frac{\omega_{i1}-\omega}{\omega-\omega_{i2}} \iff \omega = \frac{\omega'\omega_{i2}+\omega_{i1}}{\omega'+1}, \tag{6}$$

where $\omega' \in [0,\infty]$ and $\omega \in [\omega_{i1},\omega_{i2}]$. The Hamiltonian algorithm has to be applied to each $f_i(K), g(K)$ separately. It computes the function value, and the finite set of active frequencies or peaks in each window $[\omega_{i1},\omega_{i2}]$.

Subgradient information for each of the branches $f_i(K)$ is now obtained by the formulae first developed in [3] for a transfer function on the interval $[0,\infty]$. Indeed, using the change of variables (6), the ith performance channel T_i in the variable ω is transformed into a transfer function $\widetilde{T}_i$ in $\omega' \in [0,\infty]$ via

$$\widetilde{T}_i(j\omega') = \frac{1}{j\omega} \star \begin{bmatrix} \frac{\omega_{i1}}{j\omega_{i2}} & \alpha_i \\ \alpha_i & \frac{1}{j\omega_{i2}} \end{bmatrix} \star \begin{bmatrix} \mathcal{A}_i(K) & \mathcal{B}_i(K) \\ \mathcal{C}_i(K) & \mathcal{D}_i(K) \end{bmatrix} =: \frac{1}{j\omega'} \star \begin{bmatrix} \widetilde{\mathcal{A}}_i(K) & \widetilde{\mathcal{B}}_i(K) \\ \widetilde{\mathcal{C}}_i(K) & \widetilde{\mathcal{D}}_i(K) \end{bmatrix},$$

where $\alpha_i = \sqrt{\omega_{i2}-\omega_{i1}}/\omega_{i2}$, and where $\mathcal{A}_i(K)$ etc. are the system matrices of T_i, $\widetilde{\mathcal{A}}_i(K)$, etc. those of $\widetilde{T}_i$. Writing

$$\begin{bmatrix} [\widetilde{T}_i(K)](s') & [\widetilde{G}^i_{12}(K)](s') \\ [\widetilde{G}^i_{21}(K)](s') & \star \end{bmatrix} := \begin{bmatrix} \widetilde{\mathcal{C}}_i(K) \\ \widetilde{C}^i_2 \end{bmatrix} (sI - \widetilde{\mathcal{A}}_i(K))^{-1} \begin{bmatrix} \widetilde{\mathcal{B}}_i(K) & \widetilde{B}^i_2 \end{bmatrix} + \begin{bmatrix} \widetilde{\mathcal{D}}_i(K) & \widetilde{D}^i_{12} \\ \widetilde{D}^i_{21} & \star \end{bmatrix},$$

the subgradients of $f_i(K)$ are of the form [3]

$$\Phi^i_Y = 2 \sum_{\omega' \in \Omega'_i(K)} \mathrm{Re}\left\{ [\widetilde{G}^i_{21}(K)](j\omega')[\widetilde{T}_i(K)](j\omega')^H Q_{\omega'} Y_{\omega'} Q^H_{\omega'} [\widetilde{G}^i_{12}(K)](j\omega') \right\}^T, \tag{7}$$

where $\Omega'_i(K) \subset [0,\infty]$ is the finite set of active frequencies of the ith channel $\widetilde{T}_i$ in the transformed variable ω'. Here Q_ω is a matrix whose columns form an orthonormal basis of the eigenspace of $[\widetilde{T}_i(K)](j\omega')[\widetilde{T}_i(K)](j\omega')^H$ associated with its maximum eigenvalue, and $Y_{\omega'} \succeq 0$, $\sum_{\omega' \in \Omega'_i(K)} \mathrm{Tr}(Y_{\omega'}) = 1$. The subgradient is for convenience indexed by $Y = (Y_{\omega'} : \omega' \in \Omega'_i(K))$.

In order to compute subgradients of f, we now have to take into account which of the indices $i = 1,\ldots,N$ are active in the sense that $f_i(K) = f(K)$. Writing this set as $I(K)$, we obtain the

subgradients $\Phi_{Y,\tau} \in \partial f(K)$ as

$$\Phi_{Y,\tau} = \sum_{i \in I(K)} \tau_i \Phi_Y^i, \quad \sum_{i \in I(K)} \tau_i = 1, \tau_i \geq 0, \sum_{\omega' \in \Omega_i'(K)} \mathrm{Tr}(Y_{\omega'}^i) = 1, Y_{\omega'}^i \succeq 0. \tag{8}$$

3.2 Optimality function

Having explained in which way subgradients of the objective and constraint functions $f(K) = \max_{i=1,\ldots,N} f_i(K)$ and $g(K)$ are computed, let us now consider the program

$$\min\{f(K) : g(K) \leq 0\} \tag{9}$$

and investigate the generation of search steps. Following an idea in [17], we introduce the so-called progress function for (9):

$$F(K^+, K) = \max\{f(K^+) - f(K) - \mu g(K)_+; g(K^+) - g(K)_+\},$$

where $\mu > 0$ is some fixed parameter, and where g_+ stands for the positive part $g_+ = \max\{g, 0\}$. We think of K as the current iterate, K^+ as the next iterate or as a candidate to become the next iterate. A key advantage of the progress function formulation is to overcome the complications inherent to pure penalty approaches as developed in [5]. There is no penalty update and re-solving which reduces execution times and avoids artificial ill-conditioning. The following properties of the progress function are crucial for the understanding of our method. For a proof we refer to [6].

Lemma 1 *a) Suppose $\bar{K}$ is a local minimum of program (9), then $\bar{K}$ is also a local minimum of $F(\cdot, \bar{K})$. In particular, this implies $0 \in \partial_1 F(\bar{K}, \bar{K})$.*

b) If $\bar{K}$ satisfies the F. John necessary optimality conditions for (9), then $0 \in \partial_1 F(\bar{K}, \bar{K})$.

c) Conversely, if $0 \in \partial_1 F(\bar{K}, \bar{K})$, then $\bar{K}$ is either a F. John critical point of (9), or it is a critical point of constraint violation.

We have used ∂_1 to denote the Clarke subdifferential with respect to the first variable. Notice here that $\bar{K}$ is called a critical point of constraint violation of (9) if $g(\bar{K}) \geq 0$ and $0 \in \partial g(\bar{K})$. The

interpretation of this is as follows. If $g(\bar{K}) > 0$, the constraint is violated. Moreover, $0 \in \partial g(\bar{K})$ says that $\bar{K}$ is a local minimum (a critical point), so no progress toward the constraint can be made by moving from $\bar{K}$ to some nearby point $\bar{K} + dK$. In other words, a point with these characteristics means failure to solve program (9). The case $g(\bar{K}) = 0$, $0 \in \partial g(\bar{K})$ is of course the limiting case of the above. Here the point $\bar{K}$ is feasible, but we cannot further optimize $f(K)$ in the neighbourhood of $\bar{K}$, because the constraint will not let us move, as it becomes infeasible as soon as we try.

A consequence of Lemma 1 is that we should look for points $\bar{K}$ satisfying $0 \in \partial_1 F(\bar{K}, \bar{K})$. For this we apply some sort of linearization procedure to the functions f and g. Writing $f_i(K)$ in the form

$$f_i(K^+) = \max_{\omega \in I_i} \lambda_1([S_i(K^+)](j\omega))$$

we introduce a first-order approximation of f in the neighbourhood of K:

$$\begin{aligned}\widetilde{f}_i(K^+, K) &= \sup_{\omega \in I_i} \lambda_1([S_i(K)](j\omega) + [S_i'(K)](j\omega)(K^+ - K)) \\ &= \sup_{\omega \in I_i} \sup_{Z_{\omega,i} \in \mathbb{B}_i} Z_{\omega,i} \bullet ([S_i(K)](j\omega) + [S_i'(K)](j\omega)(K^+ - K)),\end{aligned}$$

where $[S_i'(K)](j\omega)$ is the Fréchet derivative of $[S_i(\cdot)](j\omega)$ at K, $\mathbb{B}_i = \{Z \in \mathbb{H}^{m_i} : Z \succeq 0, \mathrm{Tr}(Z) = 1\}$, and where m_i is the size of $S_i = T_i T_i^H$. Associating $\widetilde{g}$ with g in a similar fashion, we obtain a first-order approximation or linearization of $F(K^+, K)$:

$$\widetilde{F}(K^+, K) = \max \left\{ \max_{i=1,\ldots,N} \widetilde{f}_i(K^+, K) - f(K) - \mu g(K)_+; \widetilde{g}(K^+, K) - g(K)_+ \right\}.$$

Notice that $\widetilde{F}(K, K) = F(K, K)$, and that $\widetilde{F}(K^+, K)$ is close to $F(K^+, K)$ for K^+ in a neighborhood of K. Moreover, $\partial_1 \widetilde{F}(K, K) = \partial_1 F(K, K)$, so we keep looking for points $\bar{K}$ with $0 \in \partial_1 \widetilde{F}(\bar{K}, \bar{K})$. It is convenient to write $\widetilde{F}$ somewhat differently. We put

$$\alpha_i(Z_{\omega,i}, \omega) = Z_{\omega,i} \bullet [S_i(K)](j\omega) - f(K) - \mu g(K)_+, \qquad \Phi(Z_{\omega,i}, \omega) = [S_i'(K)](j\omega)^\star Z_i \tag{10}$$

for $i = 1, \ldots, N$, and

$$\alpha_{N+1}(Z_{\omega,N+1}, \omega) = Z_{\omega,N+1} \bullet [S_{N+1}(K)](j\omega) - g(K)_+, \Phi_{N+1}(Z_{\omega,N+1}, \omega) = [S'_{N+1}(K)](j\omega)^\star Z_{\omega,N+1}.$$

Then, putting $\mathcal{G} = \mathrm{co}\{(\alpha_i(Z_{\omega,i}, \omega), \Phi_i(Z_{\omega,i}, \omega)) : \omega \in I_i, Z_{\omega,i} \in \mathbb{B}_i, i = 1, \ldots, N+1\}$, we have

$$\widetilde{F}(K^+, K) = \max\{\alpha + \langle \Phi, K^+ - K\rangle : (\alpha, \Phi) \in \mathcal{G}\}.$$

Since $\mathcal{G}$ is an infinite set, our last step is now to replace it by a finitely representable (and therefore computable) approximation $\widehat{\mathcal{G}}$. This corresponds to replacing $\widetilde{F}(K^+, K)$ by the approximation $\widehat{F}(K^+, K)$ defined as

$$\widehat{F}(K^+, K) = \max\{\alpha + \langle \Phi, K^+ - K\rangle : (\alpha, \Phi) \in \widehat{\mathcal{G}}\}.$$

The role of $\widehat{\mathcal{G}}$ is to render the tangent program numerically tractable. It consists in choosing a finite set of frequencies, $\omega \in \Omega^i_e(K) \subset I_i$, and letting the $Z_{\omega,i} \in \mathbb{B}_i$ take a specific form.

We construct $\widehat{\mathcal{G}}$ as follows. Define $f_{N+1}(K) := g(K)$ and for every $i = 1, \ldots, N+1$ take the finite set $\Omega^i(K)$ of active frequencies of $f_i(K)$ at K. In other words, $f_i(K) = f_i(K, \omega)$ for $\omega \in \Omega^i(K)$. Now for every i add finitely many nearly active frequencies to those in $\Omega^i(K)$ to obtain an extended set of $\omega \in \Omega^i_e(K)$. Notice that $f_i(K, \omega) < f_i(K)$ for $\omega \in \Omega^i_e(K) \setminus \Omega^i(K)$. Now pick for each i and for every $\omega \in \Omega^i_e(K)$ an orthonormal basis $Q_{\omega,i}$ of the eigenspace of $f_i(K, \omega) = \lambda_1([S_i(K)](j\omega))$ at K, so that $\partial f_i(K, \omega) = \{[S'_i(K)](j\omega)^\star[Q_{\omega,i} Y_{\omega,i} Q^H_{\omega,i}] : Y_{\omega,i} \succeq 0, \mathrm{Tr}(Y_{\omega,i}) = 1\}$. In other words, $Z_{\omega,i} = Q_{\omega,i} Y_{\omega,i} Q^H_{\omega,i}$ reduces the degrees of freedom from $m_i(m_i+1)/2$ in the class of all $Z_{\omega,i}$ to the smaller size of $Y_{\omega,i}$. Include all these elements $\Phi = [S'_i(K)](j\omega)^\star[Q_{\omega,i} Y_{\omega,i} Q^H_{\omega,i}]$ with their corresponding terms $\alpha_i(Z_{\omega,i}, \omega)$ as in (10) among $\widehat{\mathcal{G}}$. As the matrix $Q_{\omega,i}$ is fixed, it is convenient to index these terms as $\Phi_i(Y_{\omega,i}, \omega)$ and $\alpha_i(Y_{\omega,i}, \omega)$, where $\omega \in \Omega^i_e(K)$ and $Y_{\omega,i} \succeq 0$, $\mathrm{Tr}(Y_{\omega,i}) = 1$ has the appropriate size, and $i = 1, \ldots, N+1$. The index $i = N+1$ adds the corresponding elements for the constraint g.

Having defined the approximation $\widehat{\mathcal{G}}$ and therefore $\widehat{F}(K^+, K)$, we solve the tangent program

$$\min_{dK} \widehat{F}(K + dK, K) + \frac{\delta}{2}\|dK\|^2. \tag{11}$$

The solution being dK, we check whether $K^+ = K + dK$ is acceptable. If this is not the case, we perform a backtracking linesearch until $K^+ = K + tdK$ satisfies the Armijo condition

$$F(K + tdK, K) - F(K, K) < \gamma t F'(\cdot, K)(K; dK)$$

for some fixed $0 < \gamma < 1$. The crucial facts about (11) have been established in [3], and we state them here without proof:

- As soon as the solution dK of (11) is nonzero, dK is a descent direction of $F(\cdot; K)$ at K. On the other hand, if the solution is $dK = 0$, then $0 \in \partial_1 F(K, K)$.

- The Armijo line search can be arranged to find a successful step after finitely many trials.

Notice that computing the Fréchet derivatives $[S_i'(K)](j\omega)$ and their adjoints leads exactly to the formulae (7) and (8) for the subgradients.

We end this section by explaining how (11) is solved. This program is of the form

$$\min_{dK} \max_{(\alpha,\Phi)\in\widehat{\mathcal{G}}} \alpha + \langle \Phi, dK \rangle + \frac{\delta}{2}\|dK\|^2.$$

Passing to the convex hull over $\widehat{\mathcal{G}}$ does not change the inner supremum, but allows us to interchange min and max using Fenchel duality. The then inner infimum over dK is unconstrained and can therefore be computed explicitly, yielding

$$dK = -(1/\delta)\Phi.$$

Substituting this back leads to the dual form of (9), which is

$$\max_{(\alpha,\Phi)\in\mathrm{co}(\widehat{\mathcal{G}})} \alpha - \frac{1}{2\delta}\|\Phi\|^2.$$

This may now be written more explicitly as

$$\begin{aligned}
\text{maximize} \quad & \sum_{i=1}^{N+1} \sum_{\omega\in\Omega_e^i(K)} \tau_{\omega,i}\alpha_i(Y_{\omega,i},\omega) - \frac{1}{2\delta}\left\|\sum_{i=1}^{N+1} \sum_{\omega\in\Omega_e^i(K)} \tau_{\omega,i}\Phi_i(Y_{\omega,i},\omega)\right\|^2 \\
\text{subject to} \quad & Y_{\omega,i} \succeq 0, \mathrm{Tr}(Y_{\omega,i}) = 1 \\
& \tau_{\omega,i} \geq 0, \sum_{i=1}^{N+1} \sum_{\omega\in\Omega_e^i(K)} \tau_{\omega,i} = 1.
\end{aligned}$$

Using a standard trick converting the quadratic expression into a linear matrix inequality, this may be turned into a (linear) semidefinite program.

A case of special interest is when the eigenvalue multiplicity of all the maximum eigenvalue functions equals 1. Then the program has the more convenient form

$$\begin{aligned}
\text{maximize} \quad & \sum_{i=1}^{N+1} \sum_{\omega\in\Omega_e^i(K)} \tau_{i,\omega}\alpha_i(\omega) - \frac{1}{2\delta}\left\|\sum_{i=1}^{N+1} \sum_{\omega\in\Omega_e^i(K)} \tau_{i,\omega}\Phi_i(\omega)\right\|^2 \\
\text{subject to} \quad & \tau_{i\omega} \geq 0, \sum_{i=1}^{N+1} \sum_{\omega\in\Omega_e^i(K)} \tau_{i,\omega} = 1.
\end{aligned}$$

which is the dual (concave) form of a convex quadratic program.

3.3 Algorithm

Parameters: $\delta > 0$, $0 < \beta, \gamma < 1$.

1: **Initialize**. Choose closed-loop stabilizing K^1.

2: **Stopping test**. If $0 \in \partial_1 \widehat{F}(K^j, K^j)$ then stop. Otherwise continue.

3: **Compute descent direction.** At counter j solve tangent program (11)

$$\min_{dK} \widehat{F}(K^j + dK, K^j) + \frac{\delta}{2}\|dK\|^2.$$

Solution is the search direction dK.

4: **Line search.** Find $t = \beta^\nu$, $\nu \in \mathbb{N}$, satisfying the Armijo condition

$$F(K^j + tdK, K^j) - F(K^j, K^j) \leq \gamma t F'(\cdot, K^j)(K^j, dK) < 0.$$

5: **Update**. Put $K^{j+1} = K^j + tdK$, increase counter j by 1 and loop back to step 2.

Notice that this algorithm is in the class of so-called phase-I-phase-II methods. As long as the constraint $g(K) \leq 0$ is not satisfied, the right hand term in $\widehat{F}$ is dominant and reducing $\widehat{F}$ amounts to reducing constraint violation. This is phase I, which ends successfully as soon as a feasible iterate $g(K^j) \leq 0$ has been found. Now phase II begins, and from now on iterates stay (strictly) feasible, and the objective function is minimized at each step. In that case the algorithm converges towards a critical point of (9). If $g(K^j) > 0$ for all j, then the algorithm converges to a critical point of constraint violation. In that case which occurs rarely in practice when constraints are feasible, a restart becomes necessary. Finally, we mention that if the controller is required to match a specific structure, PID, observer-based, decentralized, etc the proposed algorithm is easily adapted by applying a suitable chain rule to the subgradients [4].

Our code has been developed using Matlab. Fortran has been used for the QP code to minimize the main performance bottlenecks. Algorithm parameters which have been used in our applications are $\delta = 0.1$ for the QP subproblem, and β=0.5 and γ=1e-4 for the linesearch.

4 Numerical experiments

4.1 Power system oscillation damping

In this chapter we apply our new design technique to control the Brazilian North and South power subsystems interconnection described in [19]. The objective is to design a Power Oscillation Damping (POD) controller equipping the Thyristor Controlled Series Compensator (TCSC), which is installed at the south end of the interconnection. Its purpose is to minimize the system oscillation caused by external disturbances. This oscillation is due to a poorly-damped low-frequency swing mode, which is a characteristic of the interconnection: the so called North-South (NS) mode. The designed controller, however, must not produce large control output so as to avoid saturating TCSC components.

The block diagram representation of the interconnected NS system together with the closed-loop control configuration are shown in Figure 1. The controlled and measured output y represents the total active power deviation through the series capacitor. The external disturbance w represents the mechanical power deviation at a power plant located at the north end of the interconnection, while the TCSC control output u is the susceptance deviation.

Power system control is difficult due to the usually large dimension of the plant. Very often in practice, a low performance controller is synthesized heuristically. If a more systematic synthesis technique is to be used, model reduction has to be considered. Unfortunately, reduction schemes become critical or may fail when the system is large.

In our experiment we consider a medium-size approximation of the NS system with 90 states, corresponding to the least-damped scenario in [19]. In that scenario, the NS mode has damping ratio of 3.1% and a natural frequency of about 1.08 rad./s. The magnitudes of the two open-loop transfer functions $T_{w\to y}$ and $T_{u\to y}$ are shown in Figure 2. The open-loop power system state-space

representation is given by:

$$P(s): \qquad \begin{bmatrix} \dot{x} \\ y \end{bmatrix} = \begin{bmatrix} A & B_1 & B_2 \\ C_2 & 0 & D \end{bmatrix} \begin{bmatrix} x \\ w \\ u \end{bmatrix},$$

where the state vector $x \in \mathbb{R}^{90}$ and $w, u, y \in \mathbb{R}$. Note that the controller is computed with the assumption $D = 0$ and a loop transformation is applied afterwards since the power plant has a non-zero feedthrough term. See Figure 2.

A possible approach to damp the NS mode is to synthesize a controller minimizing the H_∞ norm of the disturbance channel $w \to y$, which is dominated by the NS mode resonance. However, the resulting controller is characterized by a pole-zero cancelation of the plant dynamics, which is clearly not acceptable when model variations are to be expected. Instead, we shall take advantage of the fact that our linear model has been obtained by modal truncation and thus has a diagonal state-space representation. In this representation, the NS mode is associated with the first two states, so the chosen approach is to minimize the H_∞ norm of a newly defined performance channel $w \to z^p$ from the disturbance to the first two states, described as:

$$P^p(s): \qquad \begin{bmatrix} \dot{x} \\ z^p \\ y \end{bmatrix} = \begin{bmatrix} A & B_1 & B_2 \\ [I_{2\times 2}\ 0] & 0 & 0 \\ C_2 & 0 & 0 \end{bmatrix} \begin{bmatrix} x \\ w \\ u \end{bmatrix}.$$

Unfortunately, controller synthesis based solely on such a criterion will lead to very large control effort saturating the TCSC. To counterbalance this effect we penalize the control effort through the channel $w \to z^u$

$$P^u(s): \qquad \begin{bmatrix} \dot{x} \\ z^u \\ y \end{bmatrix} = \begin{bmatrix} A & B_1 & B_2 \\ 0 & 0 & I \\ C_2 & 0 & 0 \end{bmatrix} \begin{bmatrix} x \\ w \\ u \end{bmatrix},$$

so that in closed-loop the transfer function $T_{w\to z^u}$ equals the transfer function $T_{w\to u}$ from the disturbance to the controller output.

Based on the synthesis models P^p and P^u, we define the set of multi-band constraints as follows:

- NS mode damping

$$\overline{\sigma}(\alpha_1 T_{w\to z^p}) \leq 1, \text{ for } \omega \in I_1 := [0.1, 10] \text{ rad./s},$$

- control effort limitation in the neighbourhood of the NS mode

$$|\alpha_2 T_{w\to z^u}| \leq 1, \text{ for } \omega \in I_2 := [0.1, 2] \text{ rad./s},$$

- control effort limitation in the very low frequency range

$$|\alpha_3 T_{w\to z^u}| \leq 1, \text{ for } \omega \in I_3 := [\text{1e-4,1e-3}] \text{ rad./s},$$

Trade-off between these constraints is made through the scalar positive weights α_1, α_2 and α_3. Notice that both models P^p and P^u have the same transfer function $T_{u\to y}$, but are measured on different frequency bands.

We impose three structural constraints on the controller. Firstly, the controller must be of reduced order, which is an important requirement given the dimension of the system. Here we have specified a 6th-order controller. Secondly, the controller is chosen strictly proper to reduce the effect of the external disturbance w. Finally, the controller must provide a washout effect in order to eliminate bias. Our final synthesized controller will then take the form

$$K(s) = \frac{s}{s+p}\hat{K}(s),$$

where $\hat{K}(s)$ is a strictly proper transfer function of order 5, and the position of the real washout pole $-p$ is also a decision variable of the nonsmooth program. We note that the frequency-domain constraint on interval I_3 is introduced in order to guarantee washout filtering level or bandwidth.

In practice, it prevents the variable p from being too small, and consequently the real washout pole from canceling the washout zero at the origin. The initial controller is selected as

$$K_0(s) = \frac{s}{(s+0.1)} \frac{10^4 s^2}{(s+3)^3 (s^2+2s+2)}.$$

The system is open-loop stable and the stability channel norm for K_0 is $\|(sI - \mathcal{A}(K))^{-1}\|_\infty$=7.4e-3. We have observed that the stability channel has little impact in this application as the constraint becomes never active. The initial stability constraint was set to a large value $\beta^{-1} = 10^9$. The weights $\alpha_1, \alpha_2, \alpha_3$ were chosen as $\{92, 1155, 4\text{e-}2\}$.

Taken together, the three performance constraints and the stability channel can be thought of as a synthesis plant counting 360 states. Despite that size, our nonsmooth algorithm finds a locally optimal solution for this problem after 20 iterations within 184 seconds cputime on a 2.8GHz Pentium processor with 1Gb RAM. The initial and final values of the band-restricted norms γ_i for each performance channel are given in Table 1, while Figure 3 traces their evolution along the iterations. We observe that the performance levels coalesce at the end of the optimization process near the achieved local minimum, a phenomenon that is typical for nonsmooth max functions. The final controller $K(s)$ is obtained as:

$$K(s) = \frac{s}{(s+0.0745)} \frac{0.4978s^4 + 32.98s^3 + 1.041e4s^2 + 562.8s + 148.8}{s^5 + 10.75s^4 + 45.04s^3 + 145s^2 + 138.5s + 113.5}.$$

	$\lvert T_{w\to z^p}\rvert_{I_1}$	$\lvert T_{w\to z^u}\rvert_{I_2}$	$\lvert T_{w\to z^u}\rvert_{I_3}$	$\lvert\lvert(sI-\mathcal{A}(K))^{-1}\rvert\rvert_\infty$
$K_0(s)$	1.4946	1.2628	0.0001	7.40e-3
$K(s)$	0.9884	0.9889	0.9887	8.5206e-3

TABLE 1: multi-band performance

The closed-loop system response to a disturbance step is shown in Figures 4 and 5, together with the same responses with the initial controller K_0, and with the controller from [19]. The NS mode has now 17.5% damping, without increasing control or system response overshoot. Figure 6 shows how the multi-band specifications shaped the closed-loop system in the frequency domain.

4.2 Line-of-Sight regulation of a flexible structure

We now consider the continuous control of the elevation axis of the telescope mock-up described in [1], consisting of a gimbal system mounted on flexural pivots. The primary objective is Line-of-Sight(LOS) regulation in an inertial reference coordinate system against motions of the supporting base.

The block diagram representation of the set-up is shown in Figure 7, where θ_s and $\dot{\theta}_s$ are the inertial position and velocity of the supporting base, θ_p, $\dot{\theta}_p$ and $\ddot{\theta}_p$ are the inertial position, velocity and acceleration of the telescope, u is the control torque, θ_p^m and $\ddot{\theta}_p^m$ are the measured inertial position and acceleration of the telescope, and $\ddot{\theta}_0$ represents the accelerometer bias. In the structural dynamic model, $g(s)$ is an identified transfer function of order 40, comprising the flexible modes of the telescope. The stiffness and friction feedbacks, k_b and f_b, model the flexible bearings. Magnitudes of the open-loop transfer functions $u \to \ddot{\theta}_p^m$ and $u \to \theta_p^m$ are shown in Figure 8.

Design specifications for this application are very demanding. In order to assure high quality LOS stabilization, the controller must achieve good disturbance rejection over a wide frequency range. Secondly, the closed-loop system must be robust to uncertainties due to the identification phase and to variations of the mechanical impedance of the supporting base. Also, accelerometer bias should be rejected. Finally, a simple low-order controller is sought to facilitate on-board implementation.

In traditional H_2 or H_∞ syntheses, performance and robustness specifications have to be gathered into a single criterion, which requires appending inputs and outputs of all channels. This introduces artificial crossed channels that do not reflect useful specifications. Since these cross channels are optimized along with the genuine interconnections, this approach increases conservatism. Also, traditional synthesis methods yield only full-order controllers, so that whenever simplicity is of prior importance, either a reduced plant model must be constructed or the controller has to be reduced afterwards. A further weakness of the classical approach is that weighting functions must be knitted to achieve flexible modes attenuation and reject the accelerometer bias.

With our proposed multi-band technique, each of the design specifications can be addressed

individually. Since the controller order and structure can be specified explicitly and are independent of the system dimension, there is no need to reduce plant or controller. The performance and robustness specifications are simply expressed through band-restricted performance constraints:

- **LOS regulation:** decoupling with respect to motions of the supporting base can be achieved by forcing the magnitude of the disturbance transfer function $T_{\theta_s \to \theta_p} = \theta_p(s)/\theta_s(s)$ to be very small on the frequency range of interest:

$$|T_{\theta_s \to \theta_p}| \leq -70 \text{ dB, for } \omega \in I_1 := [0, 2e3] \text{ rad./s.}$$

- **Robustness:** robustness to unstructured uncertainties in the intermediate frequency range is achieved by frequency shaping of the sensitivity function $\widetilde{S} = (I + KP)^{-1}$, where P is the plant in Figure 7. As is well known, the magnitude of the sensitivity function

$$\left|\widetilde{S}\right| = \left|(I + KP)^{-1}\right| = \frac{1}{|1 + KP|}$$

  represents the inverse of the distance to the critical point, so that minimizing $\left|\widetilde{S}\right|$ turns out to be equivalent to maximizing the stability margin. The associated restricted-band constraint is given as

$$|\widetilde{S}| \leq 1.5 \text{ , for } \omega \in I_2 := [10, 400] \text{ rad./s.}$$

- **Attenuation of flexible modes:** by a similar reasoning, the magnitude of the sensitivity function is limited in the frequency range of the flexible modes:

$$|\widetilde{S}| \leq 1.3 \text{ , for } \omega \in I_3 := [400, 2e4] \text{ rad./s.}$$

  However, this constraint alone is not enough to guarantee robustness with respect to variation of the flexible modes, because sensitivity reduction often induces pole-zero cancellation. This is clearly unacceptable since identified flexible modes are subject to uncertainties and also since the mechanical impedance of the supporting base may undergo large deviations. This

is taken into account by prescribing a maximum roll-off in the frequency range of interest: a channel $w \rightarrow z^u$ is defined as:

$$P^u(s): \quad \begin{bmatrix} \dot{x} \\ z^u \\ \begin{bmatrix} \theta_p^m \\ \ddot{\theta}_p^m \end{bmatrix} \end{bmatrix} = \begin{bmatrix} A & 0 & B_2 \\ 0 & 0 & 1 \\ C_2 & \begin{bmatrix} 0 \\ 1 \end{bmatrix} & D \end{bmatrix} \begin{bmatrix} x \\ w \\ u \end{bmatrix},$$

where $A \in \mathbb{R}^{45\times 45}$, in such a way that in closed-loop the channel $w \rightarrow z^u$ will be equivalent to the transfer function $\ddot{\theta}_p^m \rightarrow u$ of the controller. This is motivated by the fact that the flexible modes are relevant only through the accelerometer channel $u \rightarrow \ddot{\theta}_p^m$, as can be seen in Figure 8. Thus, robustness with regard to flexible modes can be achieved by forcing the transfer function $\ddot{\theta}_p^m \rightarrow u$ of the controller to be very small in the flexible modes frequency range:

$$|T_{w\rightarrow z^u}| \leq -50 \text{ dB, for } \omega \in I_4 := [5e2, 2e3] \text{ rad./s.}$$

We note that the above specification is equivalent to imposing a constraint directly on the controller gain, a thing which is not possible with more traditional Riccati or LMI H_∞ techniques. Such highly practical constraints are easy to handle with our nonsmooth optimization technique.

The first structural constraint imposed on the controller is its reduced order. A controller of order 14 is chosen. Secondly, the controller is forced to have a washout effect in the channel $\ddot{\theta}_p^m \rightarrow u$ in order to reject the accelerometer bias. Finally, the controller is chosen strictly proper for better disturbance attenuation.

The telescope system shown in Figure 7 has 45 states, structural and sensor dynamics included. Thus, the set comprising the 4 performance channels and the stability constraint correspond to a synthesis plant counting 225 states. The closed-loop transfer function $T_{\theta_s\rightarrow\theta_p}$ for the initial controller is depicted in Figure 10, while Figure 11 depicts the Nichols diagram for this initial

controller. Notice that it produces an almost unstable closed-loop flexible mode, although it presents good low-frequency properties. The initial and final values of the band-restricted norms γ_i for each performance channel are given in Table 2, while their evolution along the first 150 iterations is shown in Figure 9. The algorithm takes 355 iterations in 26 minutes cpu to reach a local minimum within the allowed tolerance. However, a feasible solution meeting all design constraints is already available after 175 iterations.

We observe again that the performance levels coalesce at the end of the iteration sequence, a strong indication that local optimality is reached. We also notice that the stability constraint $\|(sI - \mathcal{A}(K))^{-1}\|_\infty \leq 10^9$ is not active and can probably be removed without much harm, which if done from scratch leads to significant speed-up. Numerical experience reveals that the stability constraint is only useful for problems involving few band constraints. It can usually be discarded when a sufficiently rich set of simultaneous specifications is considered.

The final closed-loop transfer function $T_{\theta_s \to \theta_p}$ is shown in Figure 10. We observe an attenuation of 70 dB as specified. Figure 11 shows the Nichols diagram for the closed-loop system. These figures also show the closed-loop responses of a reduced 21-order model obtained by identification. The nominal and perturbed models differ significantly in the flexible modes range, Figure 12. However, since the magnitude of the transfer function $\ddot{\theta}_p^m \to u$ has been forced below -50 dB on the critical interval, and since the contribution of flexible modes through the channel $u \to \theta_p^m$ is negligible, the open-loop transfer function has magnitude always lower than unity, and the closed-loop system remains stable in both cases. See the Nichols plot in Figure 11. Figure 13 shows the gain plots of each performance channel. The verticals lines materialize the restricted frequency bands and the symbols $\times$ correspond to gridded frequencies which have been selected to construct the bundle of subgradients. Again as expected all band restricted performances were achieved in the sense that $f(K) \leq 1$, see Figure 13.

	$\lvert T_{\theta_s \to \theta_p} \rvert_{I_1}$	$\lvert \widetilde{S} \rvert_{I_2}$	$\lvert \widetilde{S} \rvert_{I_3}$	$\lvert T_{w \to z^u} \rvert_{I_4}$	$\lvert\lvert (sI - \mathcal{A}(K))^{-1} \rvert\rvert_\infty$
Initial	8.39	1.0863	24.533	51.65	548
Final	0.97966	0.98543	0.97776	0.98756	262

TABLE 2: Final multi-band performances for the telescope

Remark. We refer the reader to a specific advantage of our optimization method. The fact that some performance constraints become active at the local minimum, while others may remain inactive, conveys valuable information to the designer, which is not readily available if weighing filters are used. Moreover, even when all constraints are active, there is useful information available from the different weights of the subgradients of each constraint, which can be understood as Lagrange multipliers. They allow the designer to understand the relative importance of each constraint.

For further illustration of our method, we consider a simpler problem with a single band-restricted objective

$$f(K) := \|T_{\theta_s \to \theta_p}(K)\|_{I_1} \leq -100 \text{ dB}, \text{where } I_1 = [0, 100] \text{ rad/s}.$$

The evolution of the objective together with the normalized stability constraints $\beta \cdot \|(sI - \mathcal{A}(K))^{-1}\|_\infty$ is displayed in Figure 14. We observe that the stability constraint becomes active after 100 iterations, which justifies the proposed approach to maintain stability.

5 Conclusion

We have discussed a new nonsmooth algorithm for design problems subject to several band-restricted frequency domain constraints. It computes local solutions via the minimization of a progress function. A central strength of our formulation is to overcome the complications of pure penalty approaches in terms of running times and problem conditioning. Indeed, solutions of the original problem are obtained through a single minimization of the progress function.

Our approach is flexible because it bypasses the difficult phase of selecting weighting function, and because it allows to handle a large variety of controller structures of practical interest. Applications to a power system damping problem and to line-of-sight stabilization of a telescope system, both large scale, demonstrate that the approach is an efficient practical design tool in challenging situations.

Acknowledgement

This research was supported by grants from Agence Nationale de Recherche (ANR) under contract *Guidage*, by Fondation d'entreprise EADS under contract *Solving challenging problems in feedback control*, and by Agence Nationale de Recherche (ANR) under contract *Controvert*. The authors would like to thank Professors Paulo C. Pellanda (IME) and Nelson Martins (CEPEL) for providing the power system models and for their valuable suggestions. We also thank Professor Daniel Alazard (SUPAERO) for providing the telescope design problem.

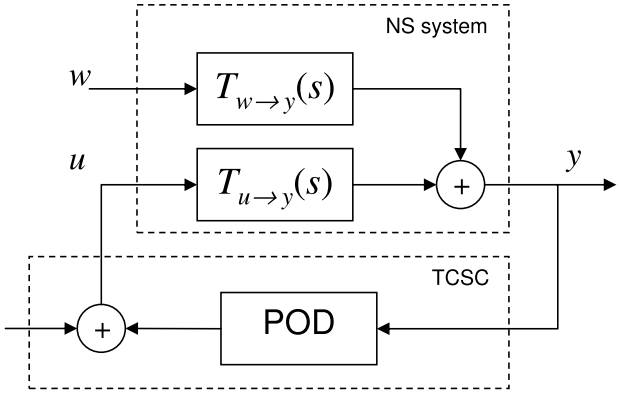

FIGURE 1: Closed-loop block diagram

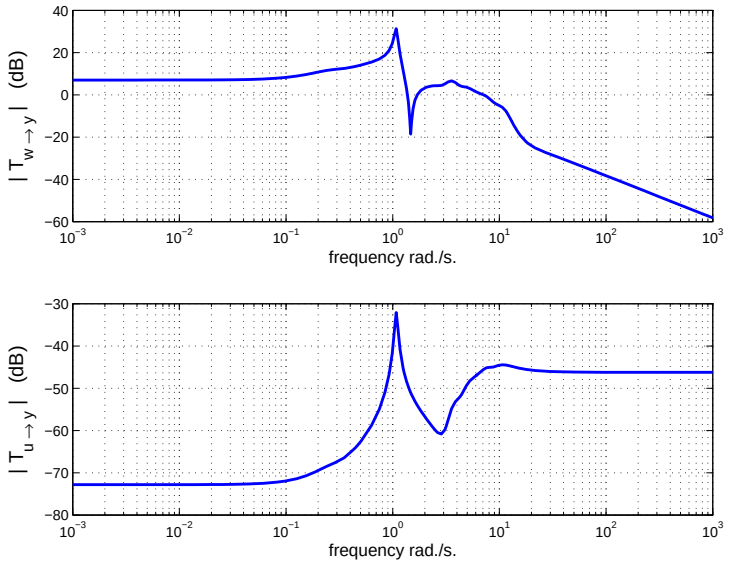

FIGURE 2: Magnitudes of open-loop transfer functions

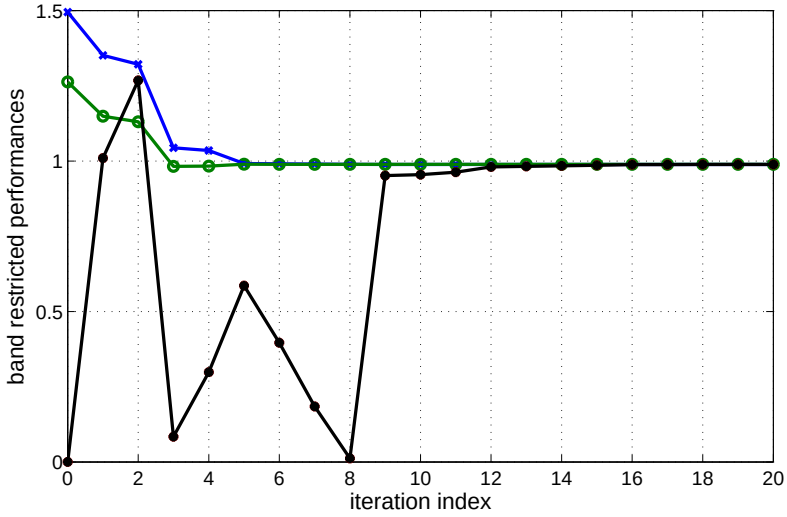

FIGURE 3: Evolution of band restricted performances vs. iteration index

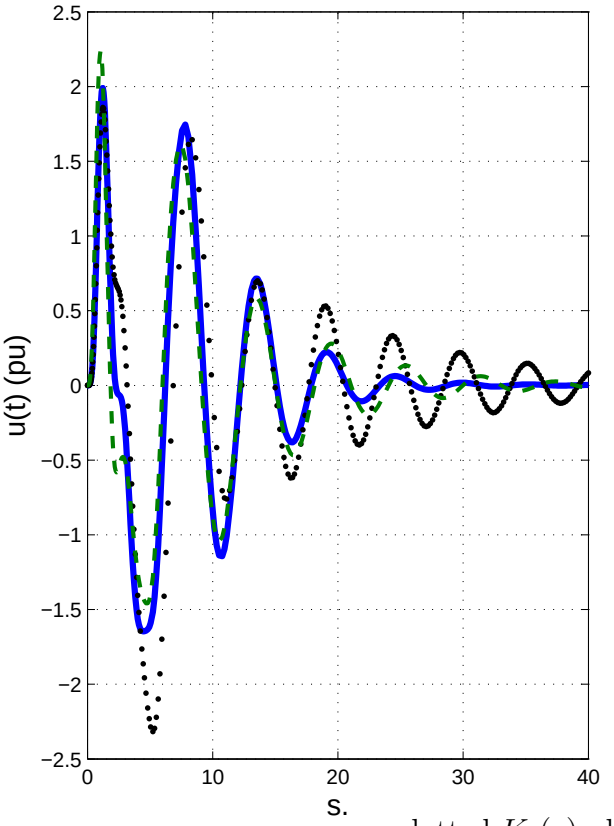

FIGURE 4: Control output step responses to disturbance

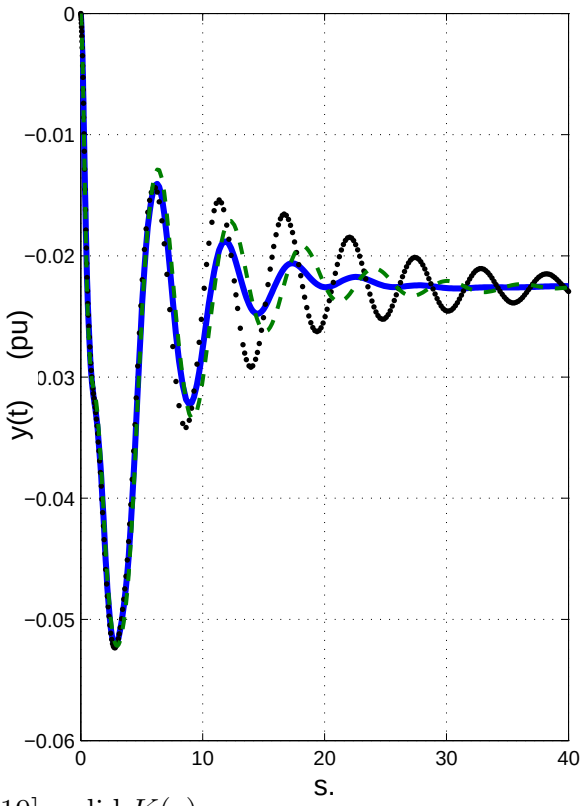

dotted:$K_0(s)$, dashed: [19], solid:$K(s)$

FIGURE 5: Output step responses to disturbance

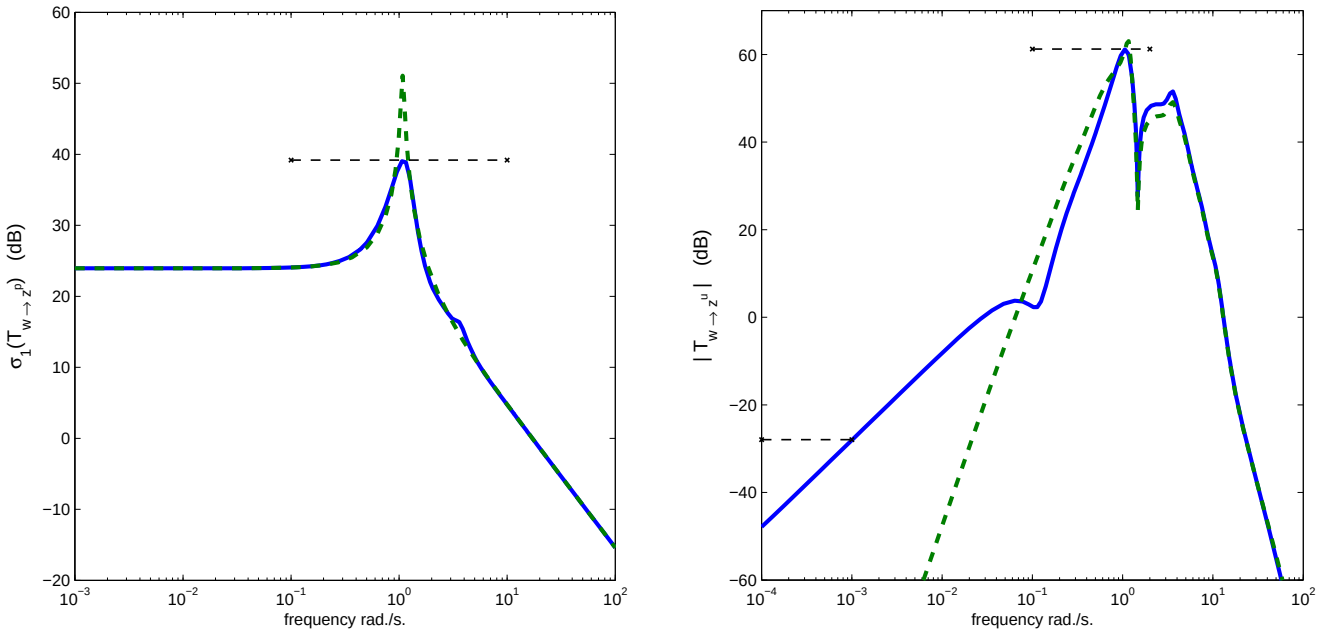

FIGURE 6: Frequency domain shaping of closed-loop system (dashed:$K_0(s)$, solid:$K(s)$)

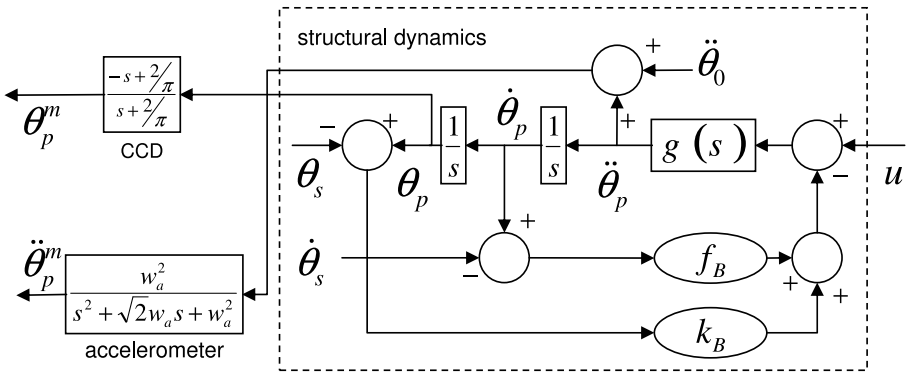

FIGURE 7: Block-diagram representation of the telescope system

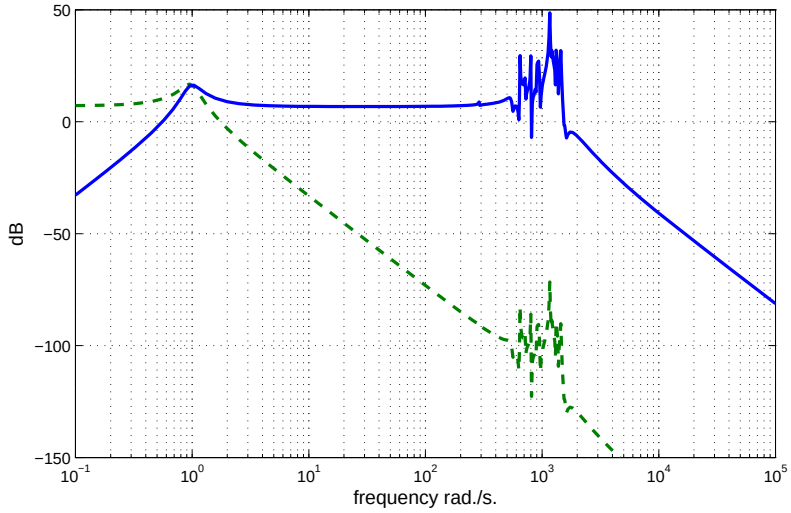

FIGURE 8: Open-loop magnitude of transfer functions $T_{u\to\ddot{\theta}_p^m}$(solid) and $T_{u\to\theta_p^m}$(dashed)

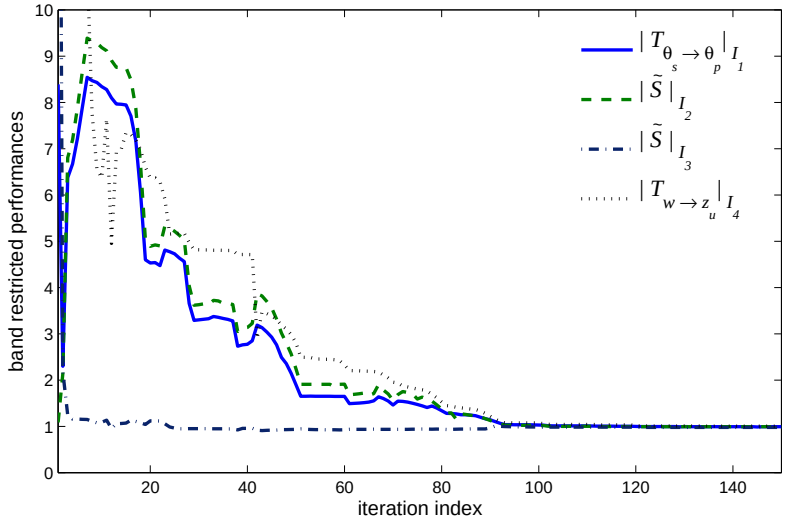

FIGURE 9: Evolution of band restricted performances vs. iteration index

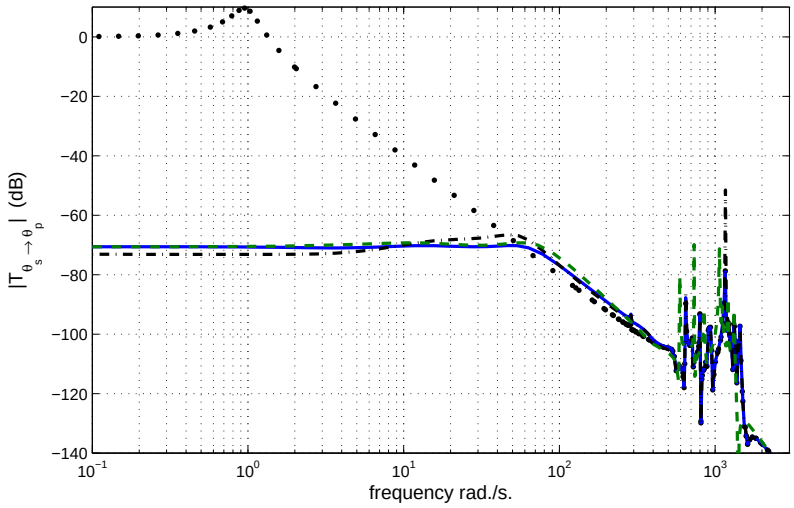

FIGURE 10: Magnitude of the transfer function $T_{\theta_s \to \theta_p}$ (solid: nominal closed-loop, dashed: perturbed closed-loop, dash-dotted: nominal open-loop, dotted: nominal with initial controller)

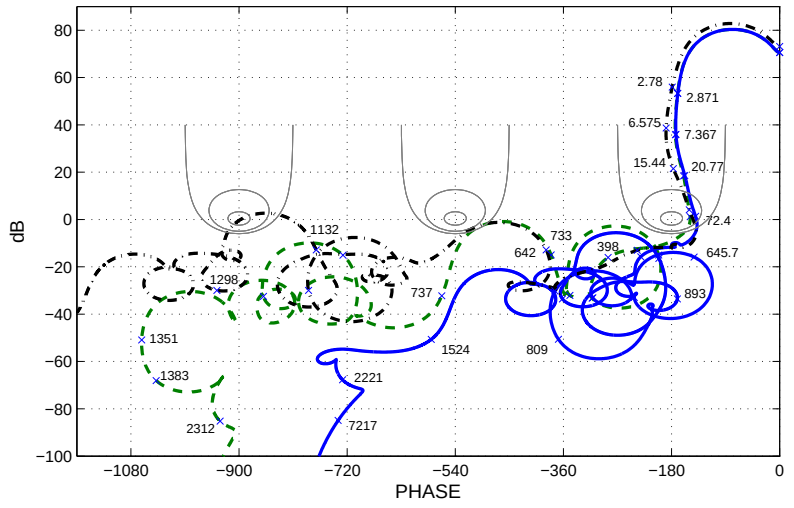

FIGURE 11: Nichols diagram (solid: final controller with nominal system, dashed: final controller with perturbed system, dash-dotted: initial controller with nominal system)

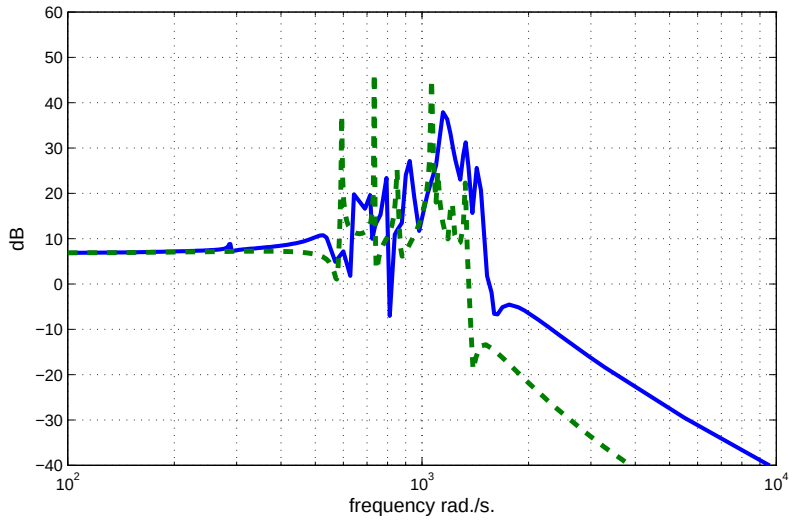

FIGURE 12: Magnitude of the open-loop transfer function $T_{u\to\ddot{\theta}_p^m}$ (solid: nominal system, dashed: perturbed system)

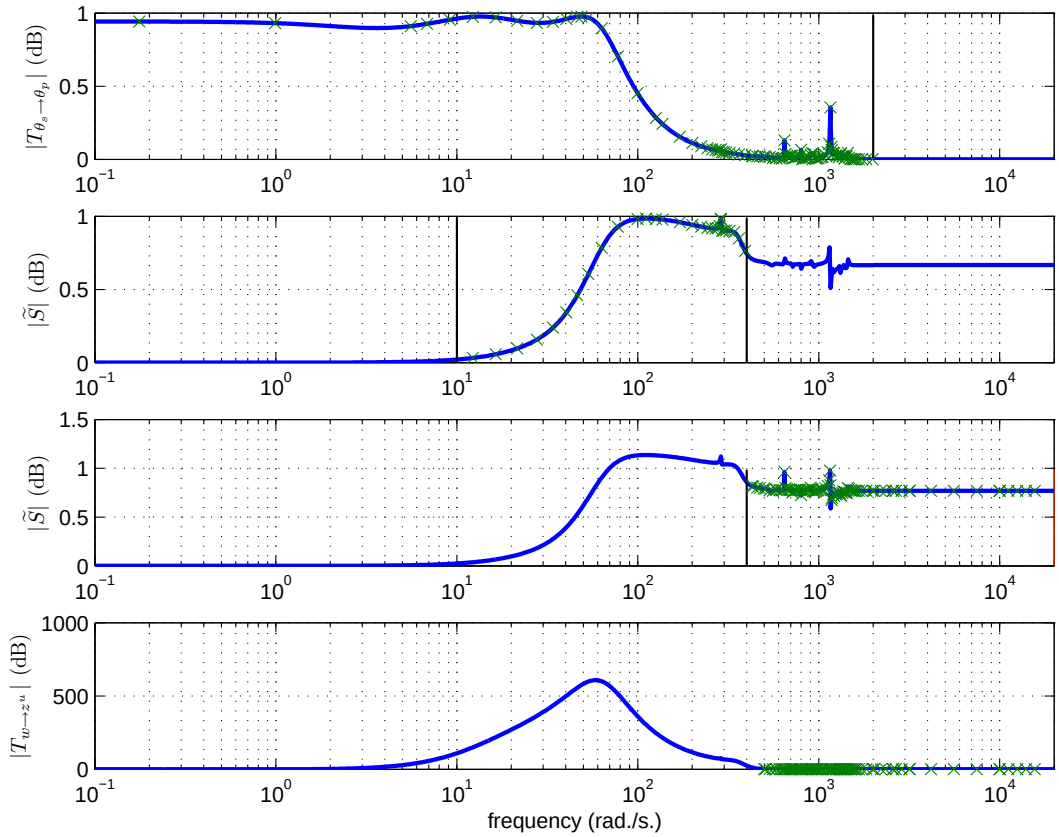

FIGURE 13: Normalized singular values of each specifications vs. frequency
× - frequency gridding

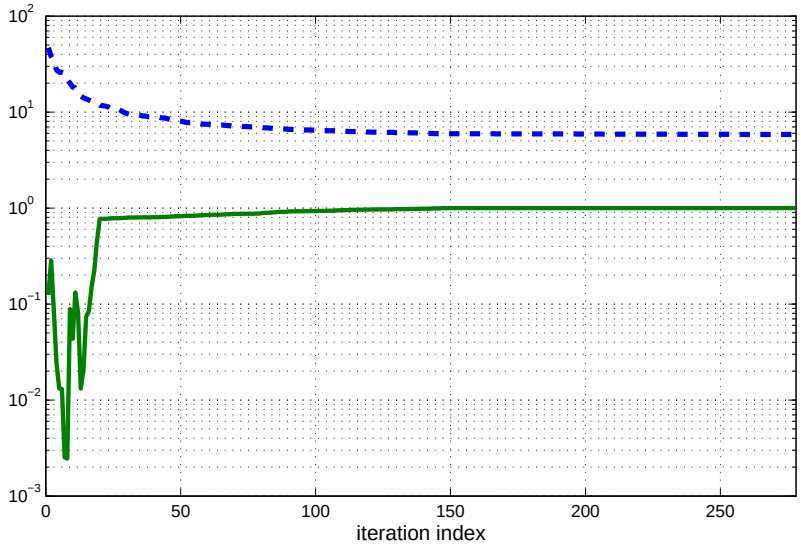

FIGURE 14: Evolution of normalized objective (dashed) and stability constraint (solid) for a simpler problem

References

[1] D. Alazard, J.P. Chrétien, and M. Le Du. Attitude control of a telescope with flexible modes. In *Dynamic and Control of Large Structures in Space*, pages 15–19, London, UK, June 1996.

[2] P. Apkarian, V. Bompart, and D. Noll. Nonsmooth structured control design with application to PID loop-shaping of a process. *Int. J. Robust and Nonlinear Control*, 17(14):1320–1342, 2007.

[3] P. Apkarian and D. Noll. Nonsmooth H_∞ synthesis. *IEEE Trans. Aut. Control*, 51(1):71–86, 2006.

[4] P. Apkarian and D. Noll. Nonsmooth optimization for multidisk H_∞ synthesis. *European J. of Control*, 12(3):229–244, 2006.

[5] P. Apkarian and D. Noll. Nonsmooth optimization for multiband frequency domain control design. *Automatica*, 43(4):724–731, April 2007.

[6] P. Apkarian, D. Noll, and A. Rondepierre. Mixed H_2/H_∞ control via nonsmooth optimization. *to appear in CDC*, 2007.

[7] H. W. Bode. *Network Analysis and Feedback Amplifier Design*. Van Nostrand, New York, 1945.

[8] S. Boyd, V. Balakrishnan, and P. Kabamba. A bisection method for computing the H_∞ norm of a transfer matrix and related problems. *Mathematics of Control, Signals, and Systems*, 2(3):207–219, 1989.

[9] S. Boyd and C. Barratt. *Linear Controller Design: Limits of Performance*. Prentice-Hall, 1991.

[10] R. Byers. A bisection method for measuring the distance of a stable matrix to the unstable matrices. *SIAM J. on Scientific and Statistical Computing*, 9:875–881, 1988.

[11] F. H. Clarke. *Optimization and Nonsmooth Analysis*. Canadian Math. Soc. Series. John Wiley & Sons, New York, 1983.

[12] G. F. Franklin, J. D. Powell, and A. Emami-Naeni. *Feedback Control of Dynamic Systems*. Prentice Hall, 2006.

[13] I. Horowitz. Quantitative feedback theory. *IEE Proc.*, 129-D(6):215–226, November 1982.

[14] T. Iwasaki and S. Hara. Generalized KYP lemma: Unified frequency domain inequalities with design applications. *IEEE Trans. Aut. Control*, 50(1):41–59, 2005.

[15] A. G. J. MacFarlane and I. Postlethwaite. The generalized Nyquist stability criterion and multivariable root loci. *Int. J. Control*, 25:81–127, 1977.

[16] D. Noll, O. Prot, and P. Apkarian. A proximity control algorithm to minimize nonsmooth and nonconvex semi-infinite maximum eigenvalue functions. *submitted*, 2007.

[17] E. Polak. *Optimization : Algorithms and Consistent Approximations*. Applied Mathematical Sciences, 1997.

[18] A. Rantzer. On the Kalman-Yacubovich-Popov Lemma. *Syst. Control Letters*, 28(1):7–10, June 1996.

[19] D. C. Savelli, P. C. Pellanda, N. Martins, N. J. P. Macedo, A. A. Barbosa, and G. S. Luz. Robust signals for the TCSC oscillation damping controllers of the brazilian north-south interconnection considering multiple power flow scenarios and external disturbances. *Proceedings of the IEEE PES General Meeting*, June 2007.

[20] H. T. Toivonen and S. Totterman. Design of fixed-structure controllers with frequency-domain criteria: a multiobjective optimisation approach. *IEE Proceedings Control Theory and Applications*, 153(1):46–52, January 2006.

[21] K. Zhou, J. C. Doyle, and K. Glover. *Robust and Optimal Control*. Printice Hall, 1996.